Stochastic Population Model for Electrical Stimulation of the Auditory Nerve

Nikita S. Imennov* and Jay T. Rubinstein, *Senior Member, IEEE*

Abstract—We have developed a biophysical model of a population of electrically stimulated auditory nerve fibers. It can be used to interpret results from physiological and behavioral experiments with cochlear implants and propose novel stimulation strategies. Our model consists of myelinated internodes described by a passive resistor–capacitor network, membrane capacitance, and leakage current at the nodes of Ranvier, as well as stochastic representations of nodal voltage-dependent channels. To approximate physiological properties measured in the auditory nerve (AN) of an acutely deafened cat, electrical parameters of the model fiber were chosen based on literature-reported values. Using our model, we have replicated the following properties within 10% of the reported [1]–[4] feline single-fiber measurements: relative spread (5.8%), spike latency (630 μs), jitter (93 μs), chronaxie (238 μs), relative refractory period (4.6 ms), and conduction velocity (14 m/s). Moreover, we have successfully matched response characteristics of a population of fibers with the same number of diameter-distributed model fibers, enabling us to simulate responses of the entire AN. To demonstrate the performance of our model, we compare responses of a population of ANs stimulated with two speech encoding strategies, Continuous Interleaved Sampling and Compressed Analog.

Index Terms—Auditory nerve (AN) fibers, cochlear implants, electrical stimulation, ion channel gating, neural prosthesis, relative spread (RS), sensory coding, stochastic ion channels, temporal jitter.

I. Introduction

ALTHOUGH speech perception among cochlear implant users has been steadily increasing over the past 25 years, many users do not achieve sentence recognition scores over 80%, and the presence of background noise further degrades their performance (cf., [5] and [6]). Laszig *et al.* have shown that binaural cochlear implants can improve sound localization and speech perception in noise [7]. However, implantees do not perform as well as normal listeners on binaural tasks, possibly because the benefits of binaural hearing depend partly on users' ability to encode interaural timing differences [8]. Improvements in encoding temporal information can overcome some of these limitations, and may also aid implantees' perception of tonal languages *via* improved pitch coding [9], and music *via* rhythm, melody, and timbre [10], [11].

To enhance our understanding of how auditory nerves (AN) encode timing, frequency, and intensity information, a number of computational models of electrically stimulated mammalian nerve fibers have been developed [12]–[17]. Deterministic models, such as the one proposed by Frijns *et al.* can predict a number of important properties, such as threshold, firing rate, and conduction velocity of an individual fiber or a population of fibers [18]. However, deterministic models fail to accurately represent the probabilistic firing of nerves, a property that has been argued to be key in describing how the AN encodes information [19]–[21].

To address this limitation, some phenomenological models (e.g., [1] and [19]) include a Gaussian noise term in calculation of the membrane current. However, axonal excitability and membrane noise concomitantly change with the state of ion channels [22], [23], which becomes particularly relevant at higher rates of stimulation [24], [25]. Therefore, to accurately describe temporal (e.g., latency) and probabilistic (e.g., relative spread (RS) and jitter) response properties of fibers, a model of electrically stimulated AN needs to represent the stochastic nature of ion channels.

To construct a robust population model of an AN, we first matched the behavior of our stochastic model to that of a single mammalian fiber. Since properties of cat AN have been extensively studied [1], [3], [26]–[28], whenever possible, we optimized our model's response to match the behavior of feline AN fibers.

Having met reported values for chronaxie, latency, jitter, and RS, we constructed a diameter-distributed population of nerve fibers, and successfully replicated an *in vivo* response of a neural population. Finally, we used our newly validated population model to simulate and visualize the response of the AN to two sound encoding strategies—Continuous Interleaved Sampling and Compressed Analog (CIS, [29] and CA, [30], respectively).

II. Methods

A. Computational Model

The spatially distributed, stochastic model used in this study is based on the morphology of a typical feline Type I spiral ganglion peripheral process, described in Table I. Implementation of the model has remained the same as reported by Mino *et al.* [35], save for the modification of model parameters to more accurately represent the behavior of a mammalian AN.

Nodes of Ranvier in a fiber consist of voltage-dependent ion channels and passive membrane components (resistance and capacitance). The number of channels at each node is calculated

TABLE I
MORPHOLOGICAL PARAMETERS OF A SINGLE MODEL FIBER

Parameter	Value	Ref.[a]
Axon diameter	1.5 μm	[31]
Axon/fiber ratio	0.6	[32], [33]
Fiber Diameter	2.5 μm	—
Nodes of Ranvier:		
Nodal length	1 μm	[34]
Constriction factor	0.5	[31]
Internodes:		
Total num.	36	
Segments per ∼	9	
Length/Diam. ratio	92 : 1	[31], [32]
Length	230 μm	—
Timestep	1 μs	

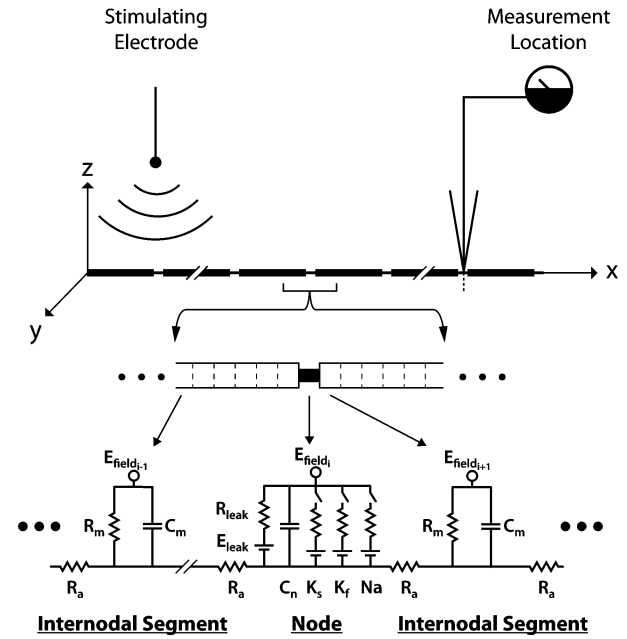[a] Values calculated from referenced quantities are indicated with a "—".

Fig. 1. Model of Type I spiral ganglion peripheral process. Note stochastic channels at nodes of Ranvier; internodes composed of identical passive-element segments. Not drawn to scale.

based on each channel's density, multiplied by the geometric surface area of the node,

$$SA_{node} = 0.5\pi \times d_{axon} \times l_{node} \qquad [\mu m]$$

where 0.5 is the constriction factor [31], d_{axon} is the axon diameter, and l_{node} is the nodal length. A Markov process was used to simulate the stochastic nature of the sodium and potassium channels, while gating parameters governing the opening and closing kinetics were chosen based on values from the biophysical literature.

Unlike the nodes of Ranvier, internodes were modeled using only passive membrane elements—resistance and capacitance. Each internode is represented by nine passive segments (see Fig. 1, "Internodal Segment" label), with total length of the internode calculated from the diameter of individual fibers. Specifically, we used a constant ratio of 92:1, measured in feline peripheral AN fibers (see "Length/Diam. ratio" entry in Table I). Since larger-diameter fibers would be longer than smaller-diameter fibers as a result of using this constant ratio, we normalized the number of internodes in a fiber such that the extent to which a fiber is simulated would be the same, regardless of its diameter (see Fig. 1). Thus, we avoid unnecessary computation by calculating response only in nodes located *before* the simulation boundary.

Parameter optimization was performed manually, in an iterative manner. First, we optimized density, conductivity, and gating of the ion channels to roughly approximate RS of the fiber and its conduction velocity. Next, we iterated over a range of literature-reported electrical parameters to approximate nodal and internodal time constants by measuring chronaxie of the model fiber. After chronaxie was judged to be close to the target value, we returned to optimizing channel parameters, this time paying attention to how *all* of the chosen measures (cf., Table V) were affected. The aforementioned steps were repeated until fiber properties were within 10% of the published values. Details of specific optimization steps are described next.

1) Optimizing Parameters of Ion Channels: In fitting our model to replicate the behavior of single fibers, we varied two parameters for every type of ion channel—its conductivity and

its density. For sodium channels, intended to model $Na_v 1.6$ currents (cf., [36]), we varied parameters within the ranges commonly reported in the literature. Due to the number of studies and a variety of experimental conditions, however, values reported for single-channel conductivity of Na (γ_{Na}) and channel density varied tremendously. Initially, we allowed the density of Na channels to vary from 700 to 2000 channels/μm^2 [37], but have found that the model was better behaved toward the lower end of the range, at 618 channels/μm^2.

Initial value for single-channel conductivity of Na was based on $\gamma_{Na} = 6.4 \pm 1$ pS [38]. However, since the original experiment was performed at 4 °C, the measurement had to be temperature adjusted to 37 °C. Temperature dependence for Na conductivity, as specified by a Q_{10} value, varies from 1.3 to 1.6 [37, p. 396], which results in a range of initial γ_{Na} values of 15.2 ± 2.4 to 30.2 ± 4.7 pS. Given the large range of γ_{Na} values, we decided to keep conductivity in our model fixed at 20 pS, as it was close to the 18 pS reported by Sigworth and Neher in cultured rat muscle cells (at 18 °C–22 °C, [39]), and close to Neumcke's measurements of $\gamma_{Na} = 17.3 \pm 2.1$ pS (mean ± SEM; ten measurements on eight fibers) in rat sciatic nerve at 20 °C [40].

Potassium current was modeled as two separate components—a fast one, K_f, intended to represent intermediate and fast K^+ channels' current (I and F channels in [41]), and a slow component K_s. Rapidly activating and transient K_f current was included in our model to shorten the relative refractory period (RRP). The delayed rectifier current of K_s, on the other hand, was included for its role in accommodation to subthreshold depolarization currents and spike-frequency adaptation processes [42].

TABLE II
GATING KINETICS

Rate Constants[a]		A^{b} (ms^{-1})	B (mV)	C (mV)	Ref.
Na	α_m	6.57	**27.4**	10.3	[46]
	β_m	0.304	-25.7	9.6	
	α_h	0.34	-114.0	11.0	
	β_h	12.6	-31.8	13.4	
K_f	α_n	0.0462	**-93.2**	1.10	[46]
	β_n	0.0824	**-76.0**	10.5	
K_s	α_s	0.3	-12.5	23.6	[46], [48]
	β_s	0.003631	-80.1	21.8	[48]

[a]All of the aforementioned values are valid at 37 °C, which in some cases necessitated adjustment of A by multiplying it with $k = Q_{10}^{(37-T_o)/10}$, where T_o is the temperature at which the original experiments were performed and Q_{10} is an appropriate temperature factor (see text).
Values in **bold** are modified from cited references (see text).

[b]Constants A, B, and C were derived from the following equations:

$$\alpha_m, \alpha_n, \alpha_s = A(E-B)/\{1-\exp[(B-E)/C]\}$$

$$\alpha_h, \beta_m, \beta_n, \beta_s = A(B-E)/\{1-\exp[(E-B)/C]\}$$

$$\beta_h = A/\{1+\exp[(B-E)/C]\}$$

where the variable E represents membrane potential in millivolts, and the rest of the variables are based on the cited references.

TABLE III
INITIAL ELECTROPHYSIOLOGICAL PARAMETERS

	Value	Ref.
Node of Ranvier:		
Resistance, r_m	$831\,\Omega\cdot mm^2$	[48], [49]
Capacitance, c_m	$2E\text{-}5\,nF/mm^2$	[50]
Na density	$700 - 2000\,chan/\mu m^2$	[37], [44]
γ_{Na}	$15 - 30\,pS/chan$	[37], [38]
K_s density	$30 - 110\,chan/\mu m^2$	[37], [41]
γ_{K_s}	$8 - 13\,pS/chan$	[43]
K_f density	—	
γ_{K_f}	$5 - 10\,pS/chan$	[47]
Internode:		
Resistance, r_{mmy}	$209E6\,\Omega\cdot mm$	[50]
Capacitance, c_{mmy}	$1.63E\text{-}9\,nF/mm$	[50]
Axoplasmic resist., R_i	$700 - 1063\,\Omega\cdot mm$	[40], [51]

The starting range for conductivity of individual slow potassium channels was based on the values measured in human axons [43]. However, since the original study was performed at 22 °C–27 °C, the reported range of 7–10 pS was temperature-corrected to 8–13 pS at 37 °C ($Q_{10} = 1.2$, [44, p. 88]). The γ_{K_s} value derived for our model lies in the middle of this starting range, at 10 pS/channel. Conductivity of slow potassium channels used in our model also fall in line with temperature-adjusted measurements reported earlier by Scholz et al.: 9.8–10.5 pS (original: $\gamma_{K_s} = 8$ pS at 24 ± 2 °C, [45]). We allowed the density of K_s channels to vary from a floor value of 30 to 110 channels/μm^2 reported in [37, p. 330] [41], and, as a result of optimization, found the values converge to 41.2E−6 channels/mm^2.

Given the lack of gating kinetics data for I and F fast potassium channels, we amalgamated these currents into one fast-acting potassium channel K_f, as has been done in [46]. However, since we did not explicitly model paranodal sections of the axon (i.e., MYSA and FLUT[1]), but instead placed K_f channels at the node of Ranvier, we used 5–10 pS as the starting range for γ_{K_f} ("I_A" in [47, p. 181]), and fixed the channel density to half of K_s's.

2) Optimizing Gating Parameters: Gating parameters governing channel kinetics were based on the values reported by Schwarz et al. [48] and McIntyre et al. [46] (see Table II). Our only modifications of the reported values were to adjust Schwarz's rate constants from 20 °C to 37 °C, and to alter half-maximal voltages for Na and K_f to reflect different ion concentrations reported in which I_{K_f} and I_{Na} were measured. Specifically, activation for Na was changed from $\alpha_m = -20.4$ to -27.4 mV, and half-maximum values for fast potassium were changed to $\alpha_n = -93.2$ mV; $\beta_n = -76.0$ mV (from -83.2 and -66.0 mV, respectively). We have found that raising α_m to -27.4 mV increased the RS of a fiber from $\sim 1.5\%$ at $\alpha_m = -20.4$ mV to $\sim 6\%$ at -27.4 mV.

3) Electrical Parameters of the Fiber: Initial values for nodal resistance and capacitance in our model were set at 831 $\Omega \cdot mm^2$ and 2E−5 nF/mm^2 ([49], [50], respectively; see Table III). After the fitting process, we found that the final value for nodal capacitance, 2.05E−5 nF/mm^2 was not significantly different from its initial value. The final value for nodal resistance, however, was ten times above its initial value, at 8310 $\Omega \cdot mm^2$. Compared to previously-reported parameters, this is approximately midway between the measurements in [48], 1625 $\Omega \cdot mm^2$, and the model value in [46], 14 286 $\Omega \cdot mm^2$. The aggregate effect of the changes to the nodal resistance and capacitance is best captured by the changes to the time constant of the nodal membrane, $\tau_m = r_m c_m$. As a result of parameter optimization, the final value of τ_m was 10.25 times its initial value.

In fitting our model to match the behavior of a mammalian fiber, we expected to modify internodal parameters the most, since the starting values were based on the data obtained from amphibian nerve fibers. We centered our estimates for internodal resistance and capacitance at 209 MΩ·mm and 1.63E−9 nF/mm, respectively, and allowed the parameters to vary within 1.5 orders of magnitude [50]. In order to replicate experimentally observed behavior of feline nerve fibers, internodal resistance of our model had to be set at six times the initial value, at 12 549 MΩ·mm, while the capacitance had to be set to 1/11th of its original value, to 1.45E−10 nF/mm. As a result of these changes, time constant of the internodal membrane, $\tau_{mmy} = r_{mmy} c_{mmy}$, has changed to approximately half of its initial value.

Surprisingly, we observed that axoplasmic resistance has a large effect on the stochastic properties of a fiber. Namely, if the rest of the parameters are fixed and R_i is raised from 733 to 1063 $\Omega \cdot mm$, jitter is significantly decreased (from 93 to ~ 5 μs), along with latency (from 630 to ~ 430 μs). Therefore, to achieve the desired latency and jitter behavior of our model fiber, the final value for R_i was set to 733 $\Omega \cdot mm$, which is at the lower end of our initial range (see Table IV).

[1]MYSA: myelin sheath attachment axon segment, FLUT: fluted paranodal axon segment, see [44, p. 22] or [46, p. 996] for more.

TABLE IV
FINAL ELECTROPHYSIOLOGICAL PARAMETERS OF TUNED MODEL

	Value	Ref.
Node of Ranvier:		
Resistance, r_m	$8310\,\Omega\cdot mm^2$	[48], [49]
Capacitance, c_m	$2.05E\text{-}5\,nF/mm^2$	[50]
Na channels:		
Eq. potential	$50\,mV$	[48]
Density	$618\,chan/\mu m^2$	
γ_{Na}	$20\,pS/chan$	
K_s channels:		
Eq. potential	$-84\,mV$	[48]
Density	$41.2\,chan/\mu m^2$	
γ_{K_s}	$10\,pS/chan$	
K_f channels:		
Eq. potential	$-84\,mV$	
Density	$20.3\,chan/\mu m^2$	
γ_{K_f}	$10\,pS/chan$	
Internode:		
Resistance, r_{mmy}	$1254E6\,\Omega\cdot mm$	
Capacitance, c_{mmy}	$1.45E\text{-}10\,nF/mm$	
Axoplasmic resist., R_i	$733\,\Omega\cdot mm$	[46], [51]
External resistance	$25\,000\,\Omega\cdot mm$	
Resting potential, E_{rest}	$-84\,mV$	[48]

B. Stimulation

Because the diameter of the modeled fiber is more than an order of magnitude smaller than the electrode-to-fiber distance, the presence of the fiber will not distort the electrical field applied by the stimulating electrode [52]. Thus, the extracellular space was modeled as a homogeneous medium with an isotropic resistivity ($\rho_{\text{ext}} = 25\,000\,\Omega\cdot mm$) in which a monopolar, spherical electrode 1 μm in radius was placed. Transmembrane voltages were calculated by solving a diffusive partial differential equation via the Crank–Nicholson method (see [35, Appendix]) with the sampling step set to 1 μs during all of our simulations.

1) Replicating Experimental Measurements: Stimuli used were identical to those in Miller *et al.*'s experiments [1], [27], [53], such that our results could be directly compared to the reported physiological measurements. In most of the cases, cathodic rectangular current pulses (39 μs; monophasic) were used, except in chronaxie calculations, where the pulsewidth was varied.

2) CIS and CA Encoding: Parameters for Continuous Interleaved Sampling (CIS) [29] and Compressed Analog (CI) [30] used in our simulation were chosen to correspond to the settings used in our psychophysical experiments with a single-channel sound processor [54]. Specifically, for CIS encoding, pulsewidth was set to 75 μs; stimulation rate was 3250 Hz; and cutoff frequencies of a bandpass filter were set to 350–5500 Hz. Given that the maximum sampling rate used in our particular single-channel sound processor (Platinum Series™ Sound Processor (PSP) by Advanced Bionics Corporation) is 11 375 Hz (=91 000 Hz/8 channels), the closest pulsewidth we could achieve to CIS' 75 μs was 88 μs with the analog encoding strategy. Analogously, the closest bandpass filter frequencies were selected when mapping the analog strategy: 250–5500 Hz. It should be noted that in our modeling simulations, we used CA

to encode the input sounds, while the behavioral experiments used a sound processor with Simultaneous Analog Stimulation (SAS), a digital, proprietary implementation of the analog CA, modified by Advanced Bionics Corporation for bipolar stimulation.

To demonstrate the differences in how CIS and CA strategies encode temporal fine structure (TFS) of a sound, we used positive and negative Schroeder phase (SP) harmonic complexes of 50 Hz as a stimulating waveform [55], [56]. We chose these specific stimuli because we have extensive behavioral response data collected from cochlear implant patients [54]. To assure that an equal amount of charge was applied in each case (CIS or CA encoded SP^+ or SP^- signal), charge-balanced, biphasic stimuli were normalized by scaling their amplitudes until the integrals of the four waveforms were equal.

C. Calculation of Fiber Properties

Whenever membrane potential at the site of the measurement electrode rose above a predefined voltage threshold (V_{th}, 50 mV above the resting potential), a spike was said to occur. By counting the number of times a spike was produced at a given intensity, we calculated the firing efficiency (FE), and by varying the intensity of the stimulus and tracking FE, we obtained the fiber's input–output function.

Single-fiber threshold was defined as the stimulus level at which the FE is 50%. Latency (the time interval between stimulus onset and generation of a spike), as well as jitter (standard deviation of spike times), were computed at each fiber's threshold levels (i.e., at 50% FE).

Relative spread, a measure of the fiber's dynamic range due to the probabilistic nature of spike generation, was computed by fitting a Gaussian cumulative distribution function (CDF) to the fiber's input–output curve. To assure an accurate fit to the data, we fit CDF only to nonzero and nonunity FE values, requiring a minimum of three data points above and three data points below the 50% FE level (typically, more than 20 points were used for each RS estimate).

Absolute and relative refractory periods (ARP and RRP, respectively) were calculated by varying the masker probe interval—first, the fiber was stimulated with a masker current (FE = 100%), followed by a second, probe impulse. By tracking the intensity of the probe impulse necessary to elicit a second action potential, we established absolute and RRPs.

Chronaxie, a reflection of the membrane's time constant, is the pulsewidth necessary to reach a current level that is twice the rheobase (i.e., twice the threshold current of an infinitely long stimulus). We measured chronaxie with a strength duration curve by varying the duration of a cathodic, monophasic stimulus from 150 to 3500 μs.

III. RESULTS

A. Single Fiber Response

A typical response of our optimized, single-fiber model is shown in Fig. 2. We have plotted the voltage at the node of Ranvier closest to the measurement location (see Fig. 1 for schematic). The amplitude of the stimulus was chosen to
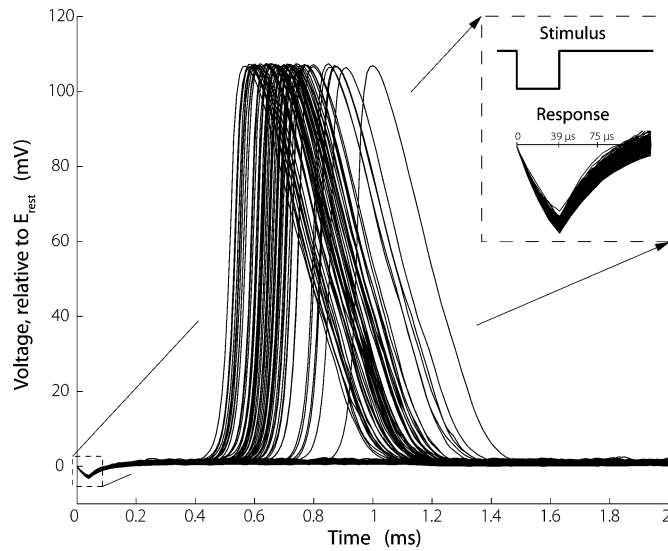
Fig. 2.   Voltage at the node of Ranvier in a single fiber (200 trials).

TABLE V
COMPARISON OF EXPERIMENTAL AND MODELED SINGLE-FIBER PROPERTIES

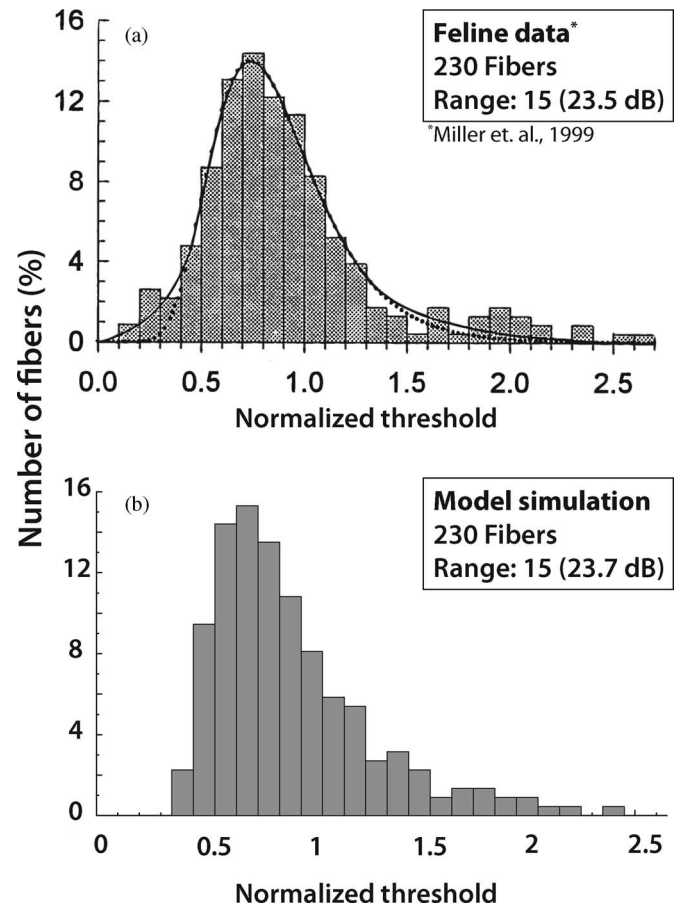| Measure	Model Fiber	% Error	Reported Values	Ref.
Relative spread	5.8%	7.9%	∼6.3%	[1]
Latency	630 μs	3.0%	∼650 μs	[1]
Jitter	93 μs	6.9%	∼100 μs	[1]
Chronaxie	238 μs	9.8%	264 μs	[2]
Cond. velocity	14 m/s		12–14 m/s	
Abs. ref. per.	**750 μs**		300–500 μs	[25], [26]
Rel. ref. per.	4.6 ms	8.0%	5 ms	[3], [4]

Fig. 3.   Comparison of (a) experimentally obtained normalized thresholds in [1] to (b) matched model response.

produce a spike 50% of the time (i.e., "at threshold," such that FE = 50%). Note how all of the fibers initially display a passive response to the cathodic stimulus (0–39 μs), but only some of the fibers produce a spike. Also note the delay ("latency") from the time the stimulus is applied at time zero to the time when majority of the fibers fire. On average, delay is 630 μs, which is close to 647 ± 142 μs (mean ± SD, $n = 146$) experimentally measured by Miller *et al.,* in [27]. In view of significant scatter, likely due to experimental error (as is pointed out in [1]), we similarly rounded 647 to 650 μs.

From Fig. 2, one can also see that there is some variability in the times at which the simulated fibers produced a spike. This variability is quantified as jitter, and in our case, is equal to 93 μs, 7% less than Miller's measurement of ∼100 μs in [1]. The rest of the single-fiber characteristics of our stochastic model are summarized in Table V. Aside from the ARP, our model approaches all of the cited parameters within 10% of the mean. Of the correctly predicted values, latency, jitter, and RS are compared to the values observed in single AN fibers of cats [1]. RS recorded by Miller *et al.* in [27] as $6.28 \pm 4.4\%$ ($n = 140$), is reported as 6.3% (as in [1]), which is 7.9% higher than our model's 5.8%. For chronaxie, we used the mean (264 ± 84 μs) of 28 measurements from a feline experiment as the target value for our model [2].

Due to a great variability in reported measurements of ARPs, we present a range of 300–500 μs as the reference values ([2], [25], and [26], respectively). Although our result of 750 μs is close to 700 μs used in [57] and the ARP measured in human ECAP data (">500 μs," [58]), it falls outside of our reference range of feline ARPs. One should note that the latest single-fiber experiments conducted by Miller *et al.* measure feline ARP as 332 ± 98 μs ($n = 20$ fibers), which suggests that the value of the ARP is at the lower end of our reference range, closer to 300 μs, rather than 500 μs [25]. Our model's prediction of the RRP of 4.6 ms, on the other hand, is fairly close to the 5 ms measured in felines [3], [4], as well as in humans, [58].

B. Population Response

To measure how well a diameter-distributed model predicts response characteristics of a population of fibers, we compared threshold distribution of 230 model fibers to the normalized thresholds observed by Miller *et al.* [1]. Diameters of the model fibers were randomly selected from a Gaussian distribution (2.0 ± 0.5 μm), parameters for which were based on the estimates of mean and standard deviation for ANs in cats [59].

As can be seen in Fig. 3, thresholds of our neural population model closely approximate the range (23.7 versus 23.5 dB) and the overall shape of the log-normal distribution measured in [1]. Such a close correspondence between physiological and simulated results suggests that a diameter-distributed model may
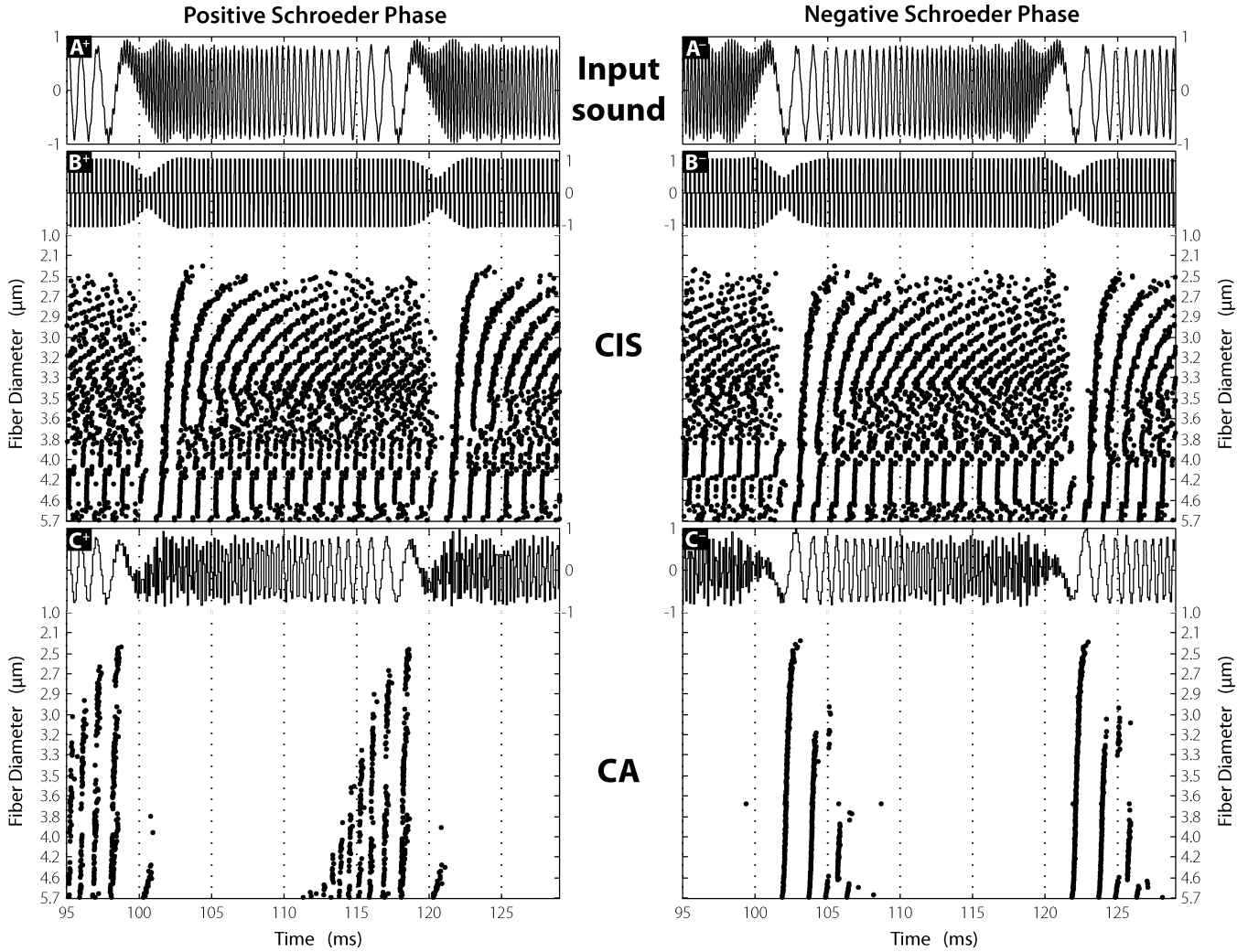
Fig. 4.   Responses of a neural population model to 50 Hz positive and negative SP input signals ($+$ and $-$, respectively). (A) Amplitudes of input signals. (B) Top panel: input sound encoded with CIS coding strategy, bottom panel: spike output of a neural population model in response to input sound encoded with CIS. (C) Same as "B", only coding was done with CA strategy.

be an adequate first-order model of excitation behavior for a population of neurons activated by a monopolar electrode.

C. Comparing Encoding Strategies

To demonstrate how a population of model fibers responds to different speech encoding strategies, we stimulated 230 fibers (the same population as in the previous section) with CA- and CIS-encoded signals ([30] and [29], respectively). As input, we used two 50 Hz Schroeder-phase signals (see "Stimulation" and Fig. 4, "Input sound" subpanels A^- and A^+). Because the envelopes of the two signals are the same, the primary difference between a positive and a negative SP complex lies in its TFS [55], [56].

Raster plots in Fig. 4 (subpanels B and C) show the times at which differently-sized fibers produced a spike. The excitation patterns shown in subpanels B^+ and B^- (CIS-encoded positive and negative SP, respectively) are fairly similar to each other. One can see that the CIS stimulus captured only the envelope of the signal; therefore, once stochasticity of the simulation is taken into account, the raster plots in B^+ and B^- are largely the same.

On the other hand, responses to CA-encoded sounds shown in subpanels C^+ and C^- are quite different from each other, with neural responses in C^+ resembling a shifted, time-reversed spike pattern seen in C^-. We provide some of the reasons as to why these two encoding strategies engender such markedly different neural responses in the discussion section next.

IV. DISCUSSION

This study described a stochastic model of the AN that faithfully reproduces the excitation characteristics of single fibers, as well as that of a population. Parameters for our model were estimated by considering measurements that have been reported in the literature as a starting point, and then refining our estimates within a reasonable range of variation. We recognize that some of the biophysical parameters in the published literature are better studied than others; therefore, our approach aimed to deviate from well-established quantities as little as possible. Additionally, to reflect the measurement error of *in vivo* data, throughout model fitting, we preferred to alter several parameters in moderation, as opposed to altering a few by a lot.

Coupled with information metrics and signal detection theory, our model can potentially be used to predict the behavioral outcomes of cochlear stimulation, thereby shortening time-consuming behavioral experiments by prescreening promising stimulation strategies during their development stages. Our immediate goal is to measure how well cochlear sound encoding strategies convey sensory information to the AN. Specifically, we plan to use results of behavioral studies (e.g., [54]) to inform us of the functional capabilities of the auditory system and information-theoretic approach to quantify the maximal amount of information contained in the neural discharge patterns (cf., [60] and [61]). In effect, the informational approach will establish the smallest degree of difference necessary for stimuli discrimination by an ideal observer, while the behavioral data will inform us how well these differences in neural response patterns are perceived by the study subjects.

As shown in behavioral studies of human listeners, internal timing structure of the auditory waveform often corresponds to the perceived qualities of pitch, timbre, and rhythm. Using the fact that different types of auditory stimuli can evoke equivalent perception of pitch, Cariani demonstrated that the intervals between spike arrival times on a feline AN correspond to the autocorrelation function of the stimulus waveform [62]. Except in cases of octave shifts, the temporal, population interval representation of pitch accounted for perception of a number of complex pitch phenomena, as well as perception of timbre characteristic of different vowel stimuli [62], [63]. This suggests that it should be possible to evaluate the relative abilities of simulated CI encoding strategies to capture sensory information such as timbre and pitch by observing their respective excitation patterns.

A. Comparing Encoding Strategies

As a proof of concept, we used our population model to simulate and visualize neural responses of 230 AN fibers to two sound encoding strategies, CIS and CA (see Fig. 4). While the differences between CIS and CA encoding strategies are well known, and CIS' inability to encode TFS is expected from first principles (e.g., compare stimuli in subpanels B^+ and B^-), this visualization is the first practical demonstration of the biophysics of TFS encoding by a cochlear implant signal processing strategy.

Of particular interest, note how the discharge patterns differ between CA-encoded positive and negative SP stimuli: in response to positive SP, spikes appear first in large-diameter fibers, later on spreading to smaller diameter fibers with correspondingly higher thresholds of excitation (e.g., $t = 112$ to 119 ms in C^+, note how it forms an "increasing triangle" pattern). Responses to negative SP exhibit the reverse trend: first, both large- and small-diameter fibers fire at the same time, with smaller fiber diameters remaining quiescent later on (e.g., the "decreasing triangle" pattern during $t = 102$ to 110 ms in C^-). Also note that excitations in response to negative SP signals occur roughly at the same time, with little temporal variability in excited fibers (see C^- at $t = 102$ and 122 ms, for example). On the other hand, responses to CA-encoded positive SP signals

display more nonuniformity, such as at $t = 98$ and 118 ms in C^+.

Even though the stimulus waveforms for the positive and negative SP stimuli look dissimilar once encoded with the CA strategy by itself, this does not imply that the listener will perceive the two sounds as being different from each other. To be perceptually relevant, the difference between the two input waveforms must be preserved at the neural level, with each type of stimulus evoking a distinct spike train. Because the model output in Fig. 4 demonstrates that the divergence between CA-encoded positive and negative SP sounds remains at the level of AN fibers, it follows that this contrast is potentially available to the auditory nervous system. We believe, it is the disparities in the neural excitation patterns that are responsible for the CI users' ability to discriminate positive from negative 50 Hz SP signals in CA–, but not CIS- encoded signals [54].

B. Limitations of the Model

There are several limitations to our model. First and foremost, we do not explicitly account for the geometric distances and the spatial distribution of the intervening tissues in our model. To model the space between the stimulating electrode and the fiber, we assume it to be an isotropic medium a given *electrical* distance away, which accounts for the resistivity and diffusivity of the intervening media. Omitting tissue inhomogeneities and interactions of the electric fields simplifies our model, although both Frijns *et al.* and Mino *et al.*, have demonstrated a spatiotemporal variation of neural excitation in response to changes in geometry of the tissues [18], [35]. As given before, our model presents an idealized case of monopolar cochlear implant stimulation, as it contains an explicit assumption of electrode-to-electrode independence.

Although our model contains slow potassium channels to account for spike-frequency adaptation and subthreshold accommodation [48], time constant of the delayed rectifier is not long enough to encompass short-term neural adaptation that occurs within first 100 to 300 ms of continuous stimulation [64]. To accurately model neural excitation in response to electrical stimulation with a typical speech encoding strategy, we need to incorporate adaptation in our model. Fortunately, adaptation to electric stimuli is the subject of recent research efforts, in part due to its relevance to speech processing in cochlear implants [65]. In the near future, we expect to add short-term adaptation to trains of electric pulses (250 to 5000 pulses/s), such as the one described by Woo *et al.*'s model in [65].

REFERENCES

[1] C. Miller, P. Abbas, and J. T. Rubinstein, "An empirically based model of the electrically evoked compound action potential," *Hear. Res.*, vol. 135, pp. 1–18, 1999.

[2] P. Stypulkowski and C. van den Honert, "Physiological properties of the electrically stimulated auditory nerve. I. Compound action potential recordings," *Hear. Res.*, vol. 14, no. 3, pp. 205–23, 1984.

[3] R. Hartmann, G. Topp, and R. Klinke, "Discharge patterns of cat primary auditory fibers with electrical stimulation of the cochlea," *Hear. Res.*, vol. 13, no. 1, pp. 47–62, 1984.

[4] S. B. C. Dynes, "Discharge characteristics of auditory nerve fibers for pulsatile electrical stimuli," Ph.D. dissertation, Massachusetts Inst. Technol., Cambridge, 1996.

[5] F.-G. Zeng, S. Rebscher, W. Harrison, X. Sun, and H. Feng, "Cochlear implants: System design, integration, and evaluation," *IEEE Rev. Biomed. Eng.*, vol. 1, pp. 115–142, 2008. Doi: 10.1109/RBME.2008.2008250

[6] B. Moore, "The role of temporal fine structure processing in pitch perception, masking, and speech perception for normal-hearing and hearing-impaired people," *J. Assoc. Res. Otolaryngol.*, vol. 9, no. 4, pp. 399–406, Dec. 2008.

[7] R. Laszig, A. Asschendorf, M. Stecker, J. Muller-Deile, S. Maune, N. Dillier, B. Weber, M. Hey, K. Begall, T. Lenarz, R. Battmer, M. Bohm, T. Steffens, J. Strutz, T. Linder, R. Probst, J. Allum, M. Westhofen, and W. Doering, "Benefits of bilateral electrical stimulation with the nucleus cochlear implant in adults: 6-month postoperative results," *Otol. Neurotol.*, vol. 25, no. 6, pp. 958–968, 2004.

[8] B. Wilson, R. Schatzer, E. Lopez-Poveda, X. Sun, D. Lawson, and R. Wolford, "Two new directions in speech processor design for cochlear implants," *Ear Hear.*, vol. 26, no. 4, pp. 73S–81S, 2005.

[9] L. Xu, Y. Tsai, and B. E. Pfingst, "Features of stimulation affecting tonal-speech perception: Implications for cochlear prostheses," *J. Acoust. Soc. Amer.*, vol. 112, no. 1, pp. 247–258, 2002.

[10] Z. M. Smith, B. Delgutte, and A. J. Oxenham, "Chimaeric sounds reveal dichotomies in auditory perception," *Nature*, vol. 416, no. 6876, pp. 87–90, 2002.

[11] Y. Kong, R. Cruz, J. Jones, and F. Zeng, "Music perception with temporal cues in acoustic and electric hearing," *Ear Hear.*, vol. 25, no. 2, pp. 173–185, 2004.

[12] F. Rattay, P. Lutter, and H. Felix, "A model of the electrically excited human cochlear neuron. I. Contribution of neural substructures to the generation and propagation of spikes," *Hear. Res.*, vol. 153, pp. 43–63, 2001.

[13] J. J. Briaire and J. H. Frijns, "The consequences of neural degeneration regarding optimal cochlear implant position in scala tympani: A model approach," *Hear. Res.*, vol. 214, no. 1–2, pp. 17–27, 2006.

[14] H. Mino, J. T. Rubinstein, and J. A. White, "Comparison of algorithms for the simulation of action potentials with stochastic sodium channels," *Ann. Biomed. Eng.*, vol. 30, pp. 578–587, 2002.

[15] O. Macherey, R. Carlyon, A. van Wieringen, and J. Wouters, "A dual-process integrator–resonator model of the electrically stimulated human auditory nerve," *J. Assoc. Res. Otolaryngol.*, vol. 8, no. 1, pp. 84–104, Mar. 2007.

[16] L. A. Cartee, "Evaluation of a model of the cochlear neural membrane. II: Comparison of model and physiological measures of membrane properties measured in response to intrameatal electrical stimulation," *Hear. Res.*, vol. 146, pp. 153–166, 2000.

[17] L. A. Cartee, "Spiral ganglion cell site of excitation. II: Numerical model analysis," *Hear. Res.*, vol. 215, no. 1–2, pp. 22–30, May 2006.

[18] J. Frijns, S. de Snoo, and R. Schoonhoven, "Potential distributions and neural excitation patterns in a rotationally symmetric model of the electrically stimulated cochlea," *Hear. Res.*, vol. 87, pp. 170–186, 1995.

[19] I. C. Bruce, M. White, L. S. Irlicht, S. O'Leary, S. Dynes, E. Javel, and G. Clark, "A stochastic model of the electrically stimulated auditory nerve: Single-pulse response," *IEEE Trans. Biomed. Eng.*, vol. 46, no. 6, pp. 617–629, Jun. 1999.

[20] E. Javel and N. Viemeister, "Stochastic properties of cat auditory nerve responses to electric and acoustic stimuli and application to intensity discrimination," *J. Acoust. Soc. Amer.*, vol. 107, no. 2, pp. 908–921, 2000.

[21] Y. Xu and L. Collins, "Predicting dynamic range and intensity discrimination for electrical pulse-train stimuli using a stochastic auditory nerve model: The effects of stimulus noise," *IEEE Trans. Biomed. Eng.*, vol. 52, no. 6, pp. 1040–1049, Jun. 2005.

[22] J. A. White, J. T. Rubinstein, and A. R. Kay, "Channel noise in neurons," *Trends Neurosci.*, vol. 23, pp. 131–137, 2000.

[23] J. T. Rubinstein, "Threshold fluctuations in an n-sodium channel model of the node of Ranvier," *Biophys. J.*, vol. 68, no. 3, pp. 779–785, 1995.

[24] A. J. Matsuoka, J. T. Rubinstein, P. J. Abbas, and C. A. Miller, "The effects of interpulse interval on stochastic properties of electrical stimulation:

Models and measurements," *IEEE Trans. Biomed. Eng.*, vol. 48, no. 4, pp. 416–424, Apr. 2001.

[25] C. A. Miller, P. J. Abbas, and B. K. Robinson, "Response properties of the refractory auditory nerve fiber," *J. Assoc. Res. Otolaryngol.*, vol. 2, pp. 216–232, 2001.

[26] C. Brown and P. Abbas, "Electrically evoked whole-nerve action potentials: Parametric data from the cat," *J. Acoust. Soc. Amer.*, vol. 88, no. 5, pp. 2205–2210, 1990.

[27] C. A. Miller, P. J. Abbas, B. K. Robinson, J. T. Rubinstein, and A. Matsuoka, "Electrically evoked single-fiber action potentials from cat: Responses to monopolar, monophasic stimulation," *Hear. Res.*, vol. 130, pp. 197–218, 1999.

[28] L. A. Cartee, C. A. Miller, and C. van den Honert, "Spiral ganglion cell site of excitation. I: Comparison of scala tympani and intrameatal electrode responses," *Hear. Res.*, vol. 215, no. 1/2, pp. 10–21, May 2006.

[29] B. S. Wilson, C. C. Finley, D. T. Lawson, R. D. Wolford, D. K. Eddington, and W. M. Rabinowitz, "Better speech recognition with cochlear implants," *Nature*, vol. 352, no. 6332, pp. 236–238, Jul. 1991.

[30] D. K. Eddington, W. H. Dobelle, D. E. Brackmann, M. G. Mladejovsky, and J. L. Parkin, "Auditory prostheses research with multiple channel intracochlear stimulation in man," *Ann. Otol. Rhinol. Laryngol.*, vol. 87, no. 6, pp. 1–39, 1978.

[31] M. Liberman and M. Oliver, "Morphometry of intracellularly labeled neurons of the auditory nerve: Correlation with functional properties," *J. Comp. Neurol.*, vol. 223, no. 2, pp. 163–176, 1984.

[32] A. R. Arnesen and K. K. Osen, "The cochlear nerve in the cat: Topography, cochleotopy, and fiber spectrum," *J. Comp. Neurol.*, vol. 178, no. 4, pp. 661–678, 1978.

[33] P. Basser, "Scaling laws for myelinated axons derived from an electrontonic core-conductor model," *J. Integr. Neurosci.*, vol. 3, no. 2, pp. 227–244, 2004.

[34] C. Berthold, "Morphology of normal peripheral axons," in *Physiology and Pathobiology of Axons*. New York: Raven, 1978, pp. 3–64.

[35] H. Mino, J. T. Rubinstein, C. A. Miller, and P. J. Abbas, "Effects of electrode–to–fiber distance on temporal neural response with electrical stimulation," *IEEE Trans. Biomed. Eng.*, vol. 51, no. 1, pp. 13–20, Jan. 2004.

[36] J. H. Caldwell, K. L. Schaller, R. S. Lasher, E. Peles, and S. R. Levinson, "Sodium channel Nav1.6 is localized at nodes of Ranvier, dendrites, and synapses," *Proc. Nat. Acad. Sci. USA*, vol. 97, no. 10, pp. 5616–5620, 2000.

[37] B. Hille, *Ion Channels of Excitable Membranes*. Sunderland, MA: Sinauer, 2001.

[38] F. J. Sigworth, "The variance of sodium current fluctuations at the node of Ranvier," *J. Physiol.*, vol. 307, pp. 97–129, 1980.

[39] F. J. Sigworth and E. Neher, "Single Na+ channel currents observed in cultured rat muscle cells," *Nature*, vol. 287, no. 5781, pp. 447–449, Oct. 1980.

[40] B. Neumcke and R. Stampfli, "Sodium currents and sodium–current fluctuations in rat myelinated nerve fibers," *J. Physiol.*, vol. 329, no. 1, pp. 163–184, 1982.

[41] B. V. Safronov, K. Kampe, and W. Vogel, "Single voltage-dependent potassium channels in rat peripheral nerve membrane," *J. Physiol.*, vol. 460, no. 1, pp. 675–691, 1993.

[42] J. R. Schwarz, G. Glassmeier, E. C. Cooper, T.-C. Kao, H. Nodera, D. Tabuena, R. Kaji, and H. Bostock, "KCNQ channels mediate IKs, a slow K+ current regulating excitability in the rat node of Ranvier," *J. Physiol.*, vol. 573, no. 1, pp. 17–34, 2006.

[43] G. Reid, A. Scholz, H. Bostock, and W. Vogel, "Human axons contain at least five types of voltage-dependent potassium channel," *J. Physiol.*, vol. 518, no. 3, pp. 681–696, 1999.

[44] S. G. Waxman, J. D. Kocsis, and P. K. Stys, *The Axon: Structure, Function, and Pathophysiology*. New York: Oxford Univ. Press, 1995.

[45] A. Scholz, G. Reid, W. Vogel, and H. Bostock, "Ion channels in human axons," *J. Neurophysiol.*, vol. 70, no. 3, pp. 1274–1279, 1993.

[46] C. McIntyre, A. Richardson, and W. Grill, "Modeling the excitability of mammalian nerve fibers: Influence of after potentials on the recovery," *J. Neurophysiol.*, vol. 87, pp. 995–1006, 2002.

[47] C. Koch and S. Idan, *Methods in Neuronal Modeling: From Ions to Networks*. Cambridge, MA: MIT Press, 1998.

[48] J. Schwarz, G. Reid, and H. Bostock, "Action potentials and membrane currents in the human node of Ranvier," *Eur. J. Physiol.*, vol. 430, pp. 283–292, 1995.

[49] T. Brismar, "Electrical properties of isolated demyelinated rat nerve fibres," *Acta Physiol. Scand.*, vol. 113, pp. 161–166, 1981.

[50] I. Tasaki, "New measurements of the capacity and the resistance of the myelin sheath and the nodal membrane of the isolated frog nerve fiber," *Amer. J. Physiol.*, vol. 181, no. 3, pp. 639–650, 1955.

[51] J. Frijns, J. Mooij, and J. ten Kate, "A quantitative approach to modeling mammalian myelinated nerve fibers for electrical prosthesis design," *IEEE Trans. Biomed. Eng.*, vol. 41, no. 6, pp. 556–566, Jun. 1994.

[52] J. T. Rubinstein, "Axon termination conditions for electrical stimulation," *IEEE Trans. Biomed. Eng.*, vol. 40, no. 7, pp. 654–663, Jul. 1993.

[53] C. A. Miller, B. Robinson, J. T. Rubinstein, P. Abbas, and C. Runge-Samuelson, "Auditory nerve responses to monophasic and biphasic stimuli," *Hear. Res.*, vol. 151, pp. 79–94, 2001.

[54] J. H. Won, W. R. Drennan, E. Jameyson, and J. T. Rubinstein, "Single-channel Schroeder phase test as a measure of within-channel temporal fine-structure sensitivity," presented at the ARO 2009 MidWinter Meeting, Baltimore, MD, Feb. 2009, poster presentation.

[55] R. J. Dooling, M. L. Dent, M. R. Leek, and O. Gleich, "Masking by harmonic complexes in birds: Behavioral thresholds and cochlear responses," *Hear. Res.*, vol. 152, pp. 159–172, 2001.

[56] W. Drennan, J. Longnion, C. Ruffin, and J. Rubinstein, "Discrimination of Schroeder phase harmonic complexes by normal-hearing and cochlear-implant listeners," *J. Assoc. Res. Otolaryngol.*, vol. 9, no. 1, pp. 138–149, 2008.

[57] L. A. Cartee, C. van den Honert, C. C. Finley, and R. L. Miller, "Evaluation of a model of the cochlear neural membrane. I: Physiological measurement of membrane characteristics in response to intrameatal electrical stimulation," *Hear. Res.*, vol. 146, no. 1–2, pp. 143–152, Aug. 2000.

[58] C. J. Brown, P. J. Abbas, and B. Gantz, "Electrically evoked whole-nerve action potentials: Data from human cochlear implant users," *J. Acoust. Soc. Amer.*, vol. 88, no. 3, pp. 1385–1391, 1990.

[59] P. Abbas and C. A. Miller, "Biophysics and physiology," in *Cochlear Implants: Auditory Prostheses and Electric Hearing* (Springer Handbook of Auditory Research), vol. 20, F. Zeng, A. Popper, and R. Fay, Eds. New York: Springer-Verlag, 2004, pp. 149–212.

[60] R. D. R. V. Steveninck and W. Bialek, "Reliability and statistical efficiency of a blowfly movement-sensitive neuron," *Philos. Trans. R. Soc. B*, vol. 348, no. 1325, pp. 321–340, 1995.

[61] Y. Xu and L. Collins, "Predictions of psychophysical measurements for sinusoidal amplitude modulated (SAM) pulse-train stimuli from a stochastic model," *IEEE Trans. Biomed. Eng.*, vol. 54, no. 8, pp. 1389–1398, Aug. 2007.

[62] P. Cariani, "Temporal coding of periodicity pitch in the auditory system: An overview," *Neural Plast.*, vol. 6, no. 4, pp. 147–172, 1999.

[63] P. Cariani, "Temporal codes, timing nets, and music perception," *J. New Music Res.*, vol. 30, no. 2, pp. 107–135, 2001.

[64] R. L. Smith, "Short–term adaptation in single auditory nerve fibers: Some poststimulatory effects," *J. Neurophysiol.*, vol. 40, no. 5, pp. 1098–1111, 1977.

[65] J. Woo, C. A. Miller, and P. J. Abbas, "Simulation of the electrically stimulated cochlear neuron: Modeling adaptation to trains of electric pulses," *IEEE Trans. Biomed. Eng.*, vol. 56, no. 5, pp. 1348–1359, May 2009.

Nikita S. Imennov received B.Sc. degrees in Biomedical Engineering (with distinction) and Computer Science (*cum laude*) from the University of Rochester, Rochester, NY, in 2004. He is currently working toward the Ph.D. degree in Bioengineering at the University of Washington, Seattle.

His current research interests include computational neuroscience, stochastic modeling, signal processing, and large-scale parallel programming.

Jay T. Rubinstein (S'80–M'82–SM'06) received the Sc.B. and Sc.M. degrees in Engineering from Brown University, Providence, RI, in 1981 and 1983, respectively, and the M.D. and Ph.D. degrees in Bioengineering from the University of Washington, Seattle, in 1987 and 1988, respectively.

In 1994, he completed postdoctoral research training and residency in Otolaryngology at the Massachusetts Eye and Ear Infirmary. During 1995, he was an Assiatant Professor and completed his Neurotology Fellowship at the University of Iowa, where he was later an Associate Professor of Otolaryngology and Bioengineering. From 2003 to 2004, he was the Boerhaave Professor at Leiden University, the Netherlands. He is currently the Virginia Merrill Bloedel Professor of Otolaryngology and Bioengineering, and the Director of the Bloedel Hearing Research Center, University of Washington.

Prof. Rubinstein is the President-Elect of the American Auditory Society, on Council of the Association for Research in Otolaryngology, and a permanent member of the Auditory Science Study Section at the National Institutes of Health.